Long-Term Interactions between the Roman City of Ostia and Its Paleomeander, Tiber Delta, Italy

Ferréol Salomon[1], Jean-Philippe Goiran[2], Simona Pannuzi[3], Hatem Djerbi[4], Carlo Rosa[5]

[1]*Archaeology, Faculty of Humanities, University of Southampton, Avenue Campus, Southampton SO17 1BF, Great Britain; ferreol.salomon@gmail.com*

[2] *Centre National de la Recherche Scientifique (CNRS), UMR 5133-Archéorient, Archéorient, UMR 5133, Maison de l'Orient et de la Méditerranée, Université de Lyon, 7 rue Raulin, 69007 Lyon, France; jean-philippe.goiran@mom.fr*

[3] *Istituto Superiore per la Conservazione ed il Restauro, Via di San Michele 23, 00153 Rome, Italy; simona.pannuzi@beniculturali.it*

[4] *Études et valorisation archéologiques Srl (Éveha), 87 avenue des bruyères, 69 150 Décines-Charpieu, France - +33(0)6 65 30 93 53 ; hatem.djerbi@eveha.fr*

[5] *Istituto Italiano di Paleontologia Umana (IsIPU), Museo Civico di Zoologia, Via Aldrovandi 18, 00197 Rome, Italy; carlorosa62@gmail.com*

Scientific editing by Jamie Woodward

Keywords: alluvial geoarchaeology, landscape evolution, paleomeander, Ostia, Tiber delta

ABSTRACT

This study examines the long term interactions between the well-known Roman city of Ostia and a river meander. Located at the mouth of the Tiber River, Ostia was a major harbor city that connected Rome to the Mediterranean Sea. Based on aerial photography

and boreholes analysis, the paleodynamics of the *Fiume Morto's* paleomeander are understood to be linked to the urban evolution of the city of Ostia. Four periods of evolution have been identified as a result of this interdisciplinary work: (1) the foundation of Ostia's urban center, in the 4th – 3rd century BC, occurred when the meander already existed; (2) between the 4th century BC and the 3rd century AD, human/environmental interactions contributed to the compound growing of the meander which possibly eroded an important Roman road linking Ostia to Rome; (3) from the Imperial period until the meander was cut off in AD 1557-1562, the constricted meander channel at the apex led to the stability of the downstream river channel; (4) the cut off of the paleomeander was completed in 1562, leading to the filling of the paleochannel. These successive phases of channel evolution mark changing fluvial risks from the Roman period to today.

INTRODUCTION

Fluvial risks considered in a long term perspective have been the focus of several studies with the development of geoarchaeology (Brown, 1997; Arnaud-Fassetta, 2008), and the results of some studies have been used to evaluate present risks in the floodplains (Bravard et al., 2008). It is important to recognize that the current concept of risk takes on different meaning depending on the cultures and the periods considered (Kasperson et al., 2005; Arnaud-Fassetta et al., 2009; Bradford et al., 2012). As such, since the 1980's, interdisciplinary studies involving archaeologists, geoarchaeologists and historians have been engaged to examine possible alluvial risks during the Roman period to cities (Bravard, Burnouf, & Vérot, 1989; Bravard et al., 1990; Allinne, 2007; Leveau, 2008; Arnaud-Fassetta et al., 2010) and deltaic areas (Arnaud-Fassetta & Landuré, 2003). During the Roman period,

the term “risk” did not exist, but the experience of fluvial events and their disruptions in Rome are well recorded in ancient texts (Le Gall, 1953). At the beginning of the 1st century AD, Romans even considered several plans in the watershed of the Tiber River to prevent or reduce the floods in Rome (Leveau, 2008).

In this context, the study of the relationship between the Roman site of Ostia, located 20 km downstream of Rome, and the Tiber River is significant to examine the risk of fluvial mobility and the modalities of its inconvenience regarding Ostia over a long period of time. Founded at the mouth of the Tiber River, Ostia was a crucial city in the Roman world and existed over at least one thousand years (6th/3rd century BC to 4th-5th century AD), with revivals in the *Borgo di Ostia* from late antiquity to the present (Figure 1). Today, Ostia is one of the most extensively excavated Roman cities. Historical and archaeological scientific literature attests that Ostia was a harbor city connecting Rome to the Mediterranean Sea and that it controlled access to the Tiber River. Recently, the location of a harbor basin has been confirmed on the left bank of the Tiber at Ostia (Heinzelmann & Martin, 2002; Goiran et al., 2014; Hadler et al., 2015), but it is small in size when compared to the basins at Portus (Keay et al., 2005; Goiran et al., 2010). Considering the recent discovery of warehouses facing both sides of the river mouth (Keay, Parcak, & Strutt, 2014), it is possible that the entire Tiber channel flowing through Ostia was a linear harbor. Consequently, we can assume that the river banks and channel mobility would have been considered carefully by the Romans.

This paper looks at the development of the area of Ostia since the Roman period in correlation with the evolution of the paleomeander of Ostia. Specifically, this study will (1)

analyze the morphology of the paleomeander in detail using aerial photography, (2) provide the complete sedimentary sequence of the convexity and the cut-off channel, (3) determine the chronology of the evolution of the paleomenader and (4) put this new data into archaeological context. Finally, the changing relationship of river and city through time will provide a solid framework to discuss the evolution of the concept of fluvial risk in Central Italy.

GEOLOGICAL AND ARCHAEOLOGICAL SETTING

The Tiber river drains a watershed of 17,375 km^2 and follows a 405 km course to the Tyrrhenian Sea. From its confluence with the Paglia River to the sea (206 km), the Tiber River shows a meandering morphology. This study focuses on the deltaic plain, *ca.* 25 km downstream of Rome. The annual mean water discharge at Rome is 240 m^3/s, with the highest water discharge measured and calculated around 3100 m^3/s during a flood in 1900 (Calenda, Mancini, & Volpi, 2009). More ancient data concerning the floods is recorded through water levels (Martino & Belati, 1980) or ancient texts from the Roman period (Le Gall, 1953; Bersani & Bencivenga, 2001). Before 1950, the Tiber River was still crossed by a few dams, and the suspended matter represented 7.18 x 10^6 t/yr. Now, the suspended matter is only about 1.41 x 10^6 t/yr (Iadanza & Napolitano, 2006). The bedload discharge has been measured only once in 1990, with respect to only one medium flood event deposit (Bersani & Amici, 1993).

The Tiber Delta formation and evolution has been studied using sedimentary data since the 1980s (Bellotti et al., 1989, 1995, 2007; Milli et al., 2013). The delta developed

from 6000-4000 cal. yr BP onward (Amorosi & Milli, 2001; C. Giraudi, 2004; Bellotti et al., 2007; Milli et al., 2013; Salomon, 2013) and is composed of the upper deltaic plain (paleolagoons area), the lower deltaic plain (beach ridges area), and the subaqueous deltaic plain (lobes and prodelta). Paleoenvironmental data comes mainly from the littoral (Bellotti et al., 1995, 2007; C. Giraudi, 2004; Milli et al., 2013) or the lagoonal systems (Di Rita, Celant, & Magri, 2009; Bellotti et al., 2011; Carlo Giraudi, 2011; Vittori et al., 2015), or else from the harbor basins of Portus and Ostia (C. Giraudi, Tata, & Paroli, 2009; Goiran et al., 2010, 2014; Hadler et al., 2015), but little data available for the Tiber channel during the Holocene.

Many difficulties exist in the attempt to reconstruct the mobility of the river channels over time, thus many hypotheses of paleochannel dynamics have been suggested for the Tiber delta (Segre, 1986; C. Giraudi, Tata, & Paroli, 2009; Bellotti et al., 2011). The bedload of the Tiber River has been scarcely observed for the Late Pleistocene or the deltaic transgressive phase (Bellotti et al., 2007), and not clearly since the formation of the prograding Holocene Tiber Delta, *ca.* 8000-6000 years ago. The paleomeander of Ostia, cut off in 1557-1562 and thereafter called *Fiume Morto*, offers a good opportunity to study a late-Holocene channel of the Tiber River. The complete stratigraphic sequence has never been reconstructed, and the modalities of paleomeander evolution were avoided or only hypothesized.

Archaeological data concerning the foundation of Ostia (Zevi, 2001) and the evolution of the urban area have been collected since the 19th century, especially along the river channel (Calza et al., 1953; Pavolini, 2006). Archaeological work also focused on the *Fiume Morto* (Pellegrino, Olivanti, & Panariti, 1995; Shepherd, 2006) combined with

geoarchaeological hand corings but only down to a depth of 3-4 meters (Arnoldus-Huyzendveld & Paroli, 1995). However, the origins of Ostia and its paleomeander are still unclear. Textual tradition links the origin of Ostia to the reign of the king Ancus Martius at the end of the 7th century BC In contrast, archaeological data relating to the foundation of the *Castrum* with the *cardo* and the *decumanus* dates the origin of Ostia to the 4th – 3rd century BC (Zevi, 2001). During the Medieval period Ostia was abandoned, while a relative rejuvenation of the city occurred with the development of the *Borgo di Ostia*, located close to the paleomeander apex (Figure 2). Finally, according to the contemporary texts, an impressive summer flood initiated the cut off of the meander in 1557, completely separating it in 1562 (Bacci, 1576; Pannuzi, 2009).

METHODS

Three sediment cores have been drilled across the palaeochannel of the *Fiume Morto* using a mechanical rotary coring device and exported to the laboratory of sedimentology of the University of Lyon 2 in France (Core MO1: 12°17'59.16" E, 41°45'32.43" N, 1.79 m above sea level (a.s.l.); Core MO2: 12°18'0.46" E, 41°45'31.22" N, 1.7 m a.s.l.; and Core MO3: 12°17'55.19" E, 41°45'40.02" N, 2 m a.s.l.). The magnetic susceptibility was measured at every centimeter using a Bartington MS2E1 high-resolution surface sensor and enabled with visual recognition to define sedimentary units (Dearing, 1999). The identification of these units using the magnetic susceptibility has been used and validated for the Tiber delta in Salomon et al. (2012). Afterwards, the core sequences were sampled systematically regarding the units and the sub-units defined, in order to ensure that each strata was sampled. We extracted 36 samples for MO1, 33 samples for MO2, and 33 samples from

MO3. The organic material was measured by loss-on-ignition on a fraction of 10 g of raw, dry sediment placed at 375°C for 16 hours (Ball, 1964), in order to give an estimation of the productivity of the overlying water column and the sedimentation rate in fine deposits (Doyle & Garrels, 1985). The texture diagram (inorganic, organic and shell fractions) was made based on a fraction of 30 g of dry raw sediments. The coarse fraction (> 2 mm), sands (2 mm at 63 µm) and silts/clays (< 63 µm) were differentiated by weighing the sieve contents. A selection of the most representative samples of each unit was undertaken for particle-size distribution analysis. Laser granulometry was carried out using a Malvern Mastersizer 2000, on clay, silts and sands after treatments with H_2O_2 for the destruction of the organic matter and KCl for the elimination of the flocculation ions (Ca^{2+}). It provides information on the distribution of grain sizes and enables evaluation of hydrodynamic intensity (Folk and Ward, 1957; Cailleux and Tricart, 1959). Shells fragments were identified and provide information on the paleoenvironments (Perès & Picard, 1964). Radiocarbon dates were established using the accelerator mass spectrometry (AMS) method and calibrated as described by Reimer et al. (Reimer et al., 2013) (Table I). Eleven ceramics were studied by S. Zampini (pers. com.), but most of them were too small and damaged to be identified and dated (Table I).

Concerning the photo interpretation, the background of Figure 2 is created with geographical information system software that combines the topographic map of the Tiber Delta (*IGM*, 1:25,000, 2005) and an aerial photograph taken by balloon in 1911. Main archaeological findings for our purpose have been added to Figure 2 from different kinds of published data (Calza et al., 1953; Arnoldus-Huyzendveld & Paroli, 1995; Pellegrino, Olivanti, & Panariti, 1995; Heinzelmann, 2001; Bukowiecki, Dessales, & Dubouloz, 2008; Pannuzi,

2009; Goiran et al., 2014; Keay, Parcak, & Strutt, 2014). The aerial photography shows the clearest marks of the morphology of the channel of the paleomeander of Ostia just before the cutting in 1557-1562. Theoretical lobes have been drawn on the basis of the last paleochannel feature.

RESULTS

Aerial Photography Analysis: A Compound Evolution of the Paleomeander

It is possible to recognize several steps of evolution of the Tiber River channel in Figure 2. The aerial photograph taken in 1911 shows a wide Tiber channel curve that erodes part of the archaeological site of Ostia at that time (north of the *Castrum / Capitolium*) as well as the clearest delineation of the paleochannel of the meander of Ostia just before the cutting in 1557-1562. The amplitude of this last active meander was 1700 m with a radius of 330 m for the main lobe (*L1* in figure 2). The sinuosity index has been measured at 3.63 (SI=L(Lengh of the channel) / λ(wavelength) = 4100 m/1130 m) and allows us to identify the last active meander of Ostia amongst the meanders with high sinuosity (Rosgen, 1994; Van den Berg, 1995).

A detailed observation of this paleomeander reveals morphological specificities, especially a destructive shift of the main lobe to the east. Towards the north and south, secondary lobes have also been observed. The circles in green help to highlight the compound growth of this complex paleomeander. The secondary lobe upstream (*L2*) has a radius of 210 m and the secondary lobe downstream has a smaller radius of 40 m (*L3*).

Analysis of Core MO3: Convexity of the Paleomeander of Ostia

Core MO3 was drilled in the convexity of the paleomeander of Ostia. The stratigraphy presents four mains units (Figure 3).

Unit A (13 to 11.67 m below the current Italian mean sea level at Genoa (b.s.l.))

This basal Unit A is composed of yellow laminated silty sand. The coarse fraction is 8% of the total weight of the samples analyzed and contains mostly small psephites and shell fragments. Most of the shells fragments are marine bivalves, but they cannot be identified precisely. However, some *Bittium reticulatum* living in *posidonia* or rocky coasts were identified with *Lentidium mediterraneum* living in sandy to clayey coasts close to a river mouth. The age of this deposit is attributed to the beginning of the Holocene by radiocarbon date performed on a marine shell (10,070 ± 50 ^{14}C yr B.P., 9250-8951 cal. BC, Ly-8799).

Unit B (11.67 to 1.72 m b.s.l.)

A major change in the stratigraphy occurs with Unit B, and especially B1. Coarse sand composes Subunit B1 with pebbles (40 to 70% of the total weight of the samples). Coarsest pebbles have a length of 3.5 to 4 cm (A-axis), a width of 2.5 cm (B-axis), and they are 0.4 cm thick (C-axis). The flatness index is very high, around 7.5 (Cailleux & Tricart, 1959). Subunits B2 to B6 are characterized by a alternation of very coarse sand (Unit B2), coarse sand (Units B4 and B6) and medium sand deposits (Units B3, B5). These deposits date between the 4th century BC and the 1st century BC according to two radiocarbon ages from Units B3 (Bone, 2230 ± 30 ^{14}C yr B.P., 385-204 cal. BC, Ly-8792) and B5 (Charcoal, 2120 ± 30 ^{14}C yr cal. B.P., 344-51 cal. BC, Ly-8793).

Unit C (1.72 to 1.45 m b.s.l.)

Unit C consists of sands with a high content of ceramics and mortar. A piece of mortar is identified in the stratigraphy at -1.72 to -1.70 m. At -1.60 m a *Terra sigillata* "Africana A" was identified and dated to 90-250 AD (Table I).

Unit D (1.45 m b.s.l. to 1.80 m a.s.l.)

This sedimentary unit presents bedded gray and yellow silty-clay. Unlike lower units, only 2% of this unit is composed of sand. The coarse fraction disappears and the organic matter content increases up to more than 2% of the total sample analyzed.

Analysis of Core MO1: Last Active Channel of the Ostia Paleomeander

Core MO1 was drilled into the last active channel of the Ostia paleomeander (Figure 4).

Unit A (14.69 to 14.39 m b.s.l.)

Unit A is a laminated silty-sand deposit similar to Unit A in Core MO3. The samples are composed of 70% sand, 30% silts and clays, and of only 0.5% of coarse fraction. Unidentified shells were found in this unit.

Unit B (14.39 to 10.36 m b.s.l.)

Four subunits compose the sedimentary Unit B. The bottom Subunit B1 and the top layer B4 correspond to high energy deposits of pebbles and coarse sands (1 cm x 1 cm x 0.5 cm for the coarsest pebbles). The corer drilled through two levels of volcanic tuff (-11.36 m to -11.09 m and -10.57 m to -10.37 m) included in Subunit B4. It is difficult to know if the pieces of tuff were broken

originally or during the drilling. However, no sedimentary deposits are mixed with these tuffs. These coarse deposits overlap medium sand (Subunit B2 and B3).

Unit C (10.36 to 8.62 m b.s.l.)

Unit C incorporates 95% sands (mainly coarse to very coarse sand), 2% silt and clay and 3% coarse fraction. A bone fragment has been dated to AD 1455-1635 (355 ± 25 ^{14}C yr B.P. / Ly-8041).

Unit D (8.62 m to 4.24 m b.s.l.)

From the Subunit B4 to E2, the tendency is a decrease of grain-size. Unit D consists of 92% sand at the bottom to 78% at the top. In contrast, the organic matter content grows from 1% to 2%. Unidentified ceramics and bricks were found in these deposits.

Unit E (4.24 m to 0.82 m b.s.l.)

The decrease of the grain size is confirmed in this unit. Sand fraction is only 48% of Subunit E1 and the silts and clays compose more than the half of the sediments (52%). At the top of Subunit E2, the silts and clays are 99% of the sediment content. The closure of the environment is confirmed by a higher organic matter content (up to 5%). The carbon content of vegetal matter found at -0.76m was too young to be dated (Ly-8040).

Analysis of Core MO2: Concavity of the Ostia Paleomeander

Finally, Core MO2 was drilled within the concavity of the Ostia paleomeander (Figure 5).

Unit A (13.55 m to 12.19 m b.s.l.)

This yellow laminated silty sand unit is similar to Units A in Cores MO1 and MO3. Most of the shells are unidentified, but shells living in sandy coast (*Cerastoderma edule*, *Mactra* sp., *Neverita Josephina*) and near a river mouth (*Zonites nitidus*) were observed.

Unit B (12.19 m to 9.28 m b.s.l.)

This unit is composed of an intercalation of coarse sands to pebbles. The coarsest pebbles are 2.5 (A-axis) x 2 (B-axis) x 1 (C-axis) cm, which corresponds to pebbles with a very high flatness index around 4.5 (Cailleux & Tricart, 1959).

Unit C (9.28 m to 6.76 m b.s.l.)

This unit corresponds to an intercalation of fine (96% silts and clays) and sandy (61% sand) deposits. No coarse fraction was observed. Two radiocarbon dates were obtained on a wood fragment (2160 ± 25 ^{14}C yr B.P., Ly 8044; 2035 ± 30 ^{14}C yr B.P., Ly-8780), which date the layer between the 4th century BC and the 1st century AD.

Unit D (6.76 m to 0.63 m b.s.l.)

The bottom of Unit D is composed of sand. Above this sandy layer, Unit D incorporates fine particles with 92% silts and clays, 6% sands and 2% coarse fraction. Unlike the lower units, the organic matter increases up to 10%. A piece of wood collected at the top of Unit E was too young to be dated by radiocarbon (Ly-8788).

DISCUSSION

Sedimentological Characteristics and Chronology of the Paleomeander

Photo interpretation draws a relative chronological framework for this study. It is possible to hypothesize a first phase of evolution of the meander toward the east, followed by the growing of two secondary lobes toward the north and toward the south. The last step of evolution of the meander happens with the cut-off of the paleomeander in 1557-1562. Thus, the core sequences can be better understood in these phases of evolution.

At the base of the three core sequences drilled in the *Fiume Morto*, the very well sorted yellow laminated silty sand (Units A in Cores MO1, 2 and 3) (Figures 3 to 6) has been interpreted such as coastal sand from the last transgressive period when the coastline was moving up toward the east (Bellotti et al., 2007; Milli et al., 2013). Some marine shells have been preserved in this coastal sediment, of which one shell has been dated to 9250-8875 cal. BC (Ly-8799).

A sharp discontinuity on the top of these sandy sediments is observed. The stratigraphic Unit A is overlapped by pebbles and very coarse deposits from the bedload of the Tiber River (Subunits B1 in Cores MO1, 2 and 3 and also B4 in MO1). For the first time, the bedload of the Tiber river in the delta was recorded and measured, which noted a high energy deltaic river channel. Medians of these deposits fluctuated between 0.58 mm and 1.6 mm with the largest pebbles measuring A-axis=3.5 cm and B-axis=2.5 cm in MO3-Unit B1, 2.5 cm and 2 cm in MO2-Unit B1 and only 1 cm and 1 cm in MO1-Unit B4. Usually, large Mediterranean deltas have sandy river mouths (Anwar, El Askary, & Frihy, 1984; Maillet, 2005), but it is possible to find pebbles such as those in the mouth of the Rhone Delta (Arnaud-Fassetta, Quisserne, & Antonelli, 2003). These pebbles reveal major floods to torrential behaviors of the Tiber River from the late 1st millennium BC until its cut off

(Bersani, 2004). A hypothesis is that these flat pebbles, similar to coastal pebbles, have been reworked and come from an area just upstream of the Tiber delta, where similar material has been observed in the Pleistocene deltaic deposits (*Ponte Galeria* formation) (Milli, 1997). The maximum depths of these paleochannels recorded by the cores are the following: 11.70 m b.s.l. (Core MO3), 14.40 m b.s.l. (Core MO1) and 12.20 m b.s.l (Core MO2). However, it has to be taken into consideration that the ancient sea level was 80 cm below the current level during the 4th-5th century AD at Portus (Goiran et al., 2009) and probably even lower in previous centuries.

Core MO3 was drilled within the convexity of the main lobe (Figures 3 & 6). It therefore contains sediments related to the migration of the Ostia paleomeander towards the east. Fluvial deposits have been separated into three main units. First, Unit B is composed of six subunits dated to between the 4th and the 1st century BC (Ly-8792; Ly-8793). The common facies of the six subunits is the fluvial dark gray coarse sediments. They are interrupted by Subunit B3 with medium sand and a gray silty clay layer. Units B2 to B6 correspond to fluvial point bar deposits, in other words the building of the meander convexity. Unit C corresponds to medium to fine sand deposits. A pottery sherd of *terra sigillata* "*Africana A*" was found in this layer and provides a limiting age *(terminus post quem*) to the deposit. This ceramic dates the layer to around 90-250 AD. This layer reveals the beginning of Roman activity on the river bank soon after the point bar deposits accumulated on the inside of the meander channel. At the top of the core, Unit D is a bedded gray-yellow silty clay layer interpreted as a floodplain deposit. The bottom of this unit (1.35 m b.s.l.) is dated between AD 1212 and 1280 (Ly-8781).

Cores MO1 and MO2 are located within the concavity of the southern secondary lobe of the paleomeander (Figures 4, 5 and 6). Core MO1 is in the middle of the last active channel dated to AD 1557, just before the cutting. Unit B contains four subunits composed of medium sand to pebbles. Two layers of volcanic tuff fragments have been found in Subunit B4 at 11.36-11.10 m and 10.57-10.37 m. Fragments of terrestrial shells were collected in this subunit and suggest that this layer with fluvial deposits and tuff was partially formed by the erosion of a close riverbank. Subunits B2 and 3 are interpreted either as fluvial deposits or as old coastal deposits eroded and trapped below the tuff layers and the coarse bedload. From Unit C to Unit E, we can observe a decrease in the grain size. We observe very coarse deposits in Unit C, medium and silty sand in Unit D and clayey silt and silty clay in Unit E. A piece of bone found in Unit C has been dated to AD 1455-1635 (Lyon-8041). We consider Unit C as the last bedload of the Tiber river before the meander cut off, and Units D and E as the subsequent channel infill from AD 1557 onwards. As previously expressed, Unit B in Core MO2 represents bedload. This unit is covered by different types of facies (sandy and silty clay / Unit C) dated by a fragment of bone to 4th century BC – 1st century AD. Silt and clay might be deposited decantation in a period of low energy (Seasonal? Over several years?). Flocculation could have been active with the intrusion of salt water in the Tiber river channel (Capelli & Mazza, 2008). The sandy layers can be attributed either to fluvial deposits or to erosion of the river banks' coastal sands. Unit D is considered a post-cut off deposit related to the last bedload at the bottom (sandy layer), and to an oxbow lake existing until the end of the 19th century AD, after which it was finally reclaimed (Amenduni, 1884). A pollen analysis on Core MO-2 supports this interpretation (Pepe et al., 2016).

Sedimentological Data in their Archaeological and Paleoclimatic Contexts

Four main phases of evolution of the active meander of Ostia can be observed (Figure 7). The first phase corresponds to the origin of the paleomeander. The oldest sedimentary data comes from the base of Core MO3 in the convexity of the main lobe of the Ostia paleomeander. Unit B is dated to the 4th – 1st century BC by radiocarbon dating. It is possible to show that the meander of Ostia was already established when the *Castrum* was built in the 4th – 3rd century BC. Combined archaeological and sedimentological data bring to light the same period of time. However, these data do not give evidence for the existence of Ostia during the reign of the king of Rome, Ancus Martius (*ca.* 642-617 BC). Neither does it give evidence for the location of the Tiber River during that period. The main lobe channel shifts toward the east from at least 385-205 BC until the 1st century AD.

The second phase corresponds to the formation of the secondary lobes. The southern secondary lobe was already in formation in the 1st century AD. Core MO2 reveals the sedimentation at the maximum southern extent of the *Fiume Morto* dated between the mid-4th century BC and the mid 1st century AD (*terminus post quem*). The chronology provided by excavated archaeological remains is comparable concerning the date of the maximum erosion of the southern secondary lobe. The construction of the aqueduct at the end of the 2nd / beginning of the 3rd century AD is the *terminus ante quem* for the paleomeander mobility toward the south, because its outline roughly follows the curve of the last channel of the meander before its cut off in AD 1557-1562.

During the third phase, archaeological evidence and sedimentological data are consistent to support a lateral stability of the southern secondary lobe channel from the 1st / 3rd century AD to the cut-off of the meander in AD 1557-1562. The cut-off of the paleomeander was initiated by a summer flash-flood in AD 1557 that also broke the *Pons Aemilius* (also called *Ponte Rotto*) in Rome. This exceptional meteorological event is recorded in texts from South France to Sicily (Bacci, 1576). Most of the 16th century is characterized in the Tiber River by rare hydrological events with sudden major summer floods (AD 1530 & AD 1557; Bersani, 2004). These records tell us about particular conditions occurring within the Tiber watershed during some decades of the Little Ice Age (Camuffo & Enzi, 1995; Camuffo et al., 2014). Afterwards, the paleomeander was slowly filled up by sediments and finally reclaimed at the end of the 19th century / beginning of the 20th century (fourth phase).

Erosion of the *Via Ostiensis*?

When the *Castrum* of Ostia was established in the 4th – 3rd century BC, two main streets of the urban area of Ostia were delineated: the *cardo* (north-south), and the *decumanus* (west-east). The *cardo* at the north of the *Capitolium* of Ostia was eroded after the cut-off of the meander in AD 1557-1562, but at this point the city of Ostia had already been abandoned for about a millennium. However, the *Via Ostiensis*, continuing off the *decumanus,* could have been eroded during antiquity, when the economic activity of Ostia was flourishing. A notable problem here is the possibility that the *Via Ostiensis* already avoided the secondary lobes of the meander during its construction. The chronology of the deposits based on radiocarbon dates is too extended in time to solve this problem. The

shifting of the Tiber to the east and the formation of the secondary lobes could have happened in the 4th century - 3rd century BC and then been followed by the construction of the road. However, the discovery of tuff in the bedload of the paleo-Tiber channel just below the theoretical position of the *Via Ostiensis* (Core MO1) could support the hypothesis of an effective erosion of the road by the Tiber River (Figures 2 & 6). The excavations undertaken across the *Via Ostiensis* near Ostia recorded a wide distribution of pieces of tuff (Calza et al., 1953). More investigation needs to be done to definitively solve this question. Similarly, the question arises concerning an aqueduct built in the 1st century AD, which was connected to a reservoir included within the city wall of Ostia. Was the first aqueduct following the hypothetical *Via Ostiensis* eroded by the paleomeander? Unfortunately, no outline of this early aqueduct has been found near Ostia. Instead there are the remains of a ”second” aqueduct dated to the 2nd – 3rd century AD with a route following the curve of the southern secondary lobe (Bukowiecki, Dessales, & Dubouloz, 2008).

Hypothesis Regarding the Compound Evolution of the Ostia Paleomeander

Two questions are therefore pending: (1) Why does the meander’s growth stop in its migration to the east? and (2) why did the southern secondary lobe show lateral stability between antiquity and AD 1557? The stability of such a lobe is surprising over almost one millennium. An answer can be found in the theoretical knowledge concerning meander dynamics (Jin & Schumm, 1986). The meander could have been blocked by cohesive silty-clayey deposits remaining from the lagoon of Ostia (limit delineated on Figures 1 & 2) and by the presence of a huge structure composed of volcanic tuff, a possible harbor installation, dating back to the early Republican period (Pavolini, 2006). This structure still remained in

the channel in AD 1557 despite the high energy of the Tiber River. These anthropic and natural obstacles could have led to the formation of secondary lobes. Later on, the effect of these obstacles could have had consequences on the resonance of the energy upstream, accelerating the migration of the upstream channel of the meander of Ostia and stabilizing the channel downstream of the obstacles. In support of this hypothesis, the outlines of paleochannels on the two parts of the neck are not symmetrical (Figure 2). The upstream curve of the paleomeander is broader than the downstream curve in the city of Ostia and the northern secondary lobe has a larger radius. Similar mechanics are observed in flume studies (Jin & Schumm, 1986).

Additionally, a possible reduction of the water energy for medium floods is conceivable since the construction of Portus in AD 42-45. Today, one-fifth of the Tiber River discharge is flowing through Fiumicino. Other canals were excavated and in use after the construction of Portus (Testaguzza, 1970; Keay et al., 2005; Salomon et al., 2014) and could have led to the decrease of the energy of the Tiber river downstream in Ostia (Figure 1).

The City of Ostia Facing River Mobility Risks during the Roman Period

From 414 BC onward, floods of the Tiber River are recorded in ancient texts for the lower Tiber valley (Le Gall, 1953; Aldrete, 2007). These records are not systematic and depend on the observations of the ancient authors as well as the preservation of the texts through time. However, floods became a major problem in Rome at the beginning of the 1st century AD, forcing the Senate to consider solutions (Miller, 1959; Leveau, 2008). Flood management through flood-relief canals is also underlined in some inscriptions from the

middle of the 1st century AD and early 2nd century AD found at Portus (Keay et al., 2005; Salomon, 2013). Overbank flooding is the main inconvenience reported during this period in Rome, rather than river mobility disruption. However, a shift in the course of a river was observed at least elsewhere during the Roman period. Ancient jurists took into account these fluvial disruptions through their consequences on land use and possession (Campbell, 2012). The present study exposes the fact that the city of Ostia faced the problem of erosion by relocating infrastructure: locally, by moving roads and the aqueduct to the south, or regionally, by the foundation of Portus, a huge harbor system indirectly linked to the fluvial system by canals flowing to the north and to the south of the harbor basins (Salomon et al. 2012, 2014). Some of these canals prevent lateral mobility by the construction of built riverbanks such as the *Canale Romano,* the *Canale Traverso* and the *Fossa Traiana,* now called Fiumicino (Testaguzza, 1970; Keay et al., 2005). They may have been conceived and used for ship unloading, but these lateral structures did in fact also prevent lateral mobility. By comparison, it is clear that the Republican structure in the north of the paleomeander played its part on the evolution of morphology of the paleomeander together with the cohesive deposits of the palaeolagoon of Ostia, and participated in crushing the apex of the meander. However, at the moment, we cannot assume that this structure was built on purpose to prevent river bank erosion.

CONCLUSION

The study of the Tiber River paleomeander in relation to the city of Ostia provides new data to investigate long term interaction between human settlements and fluvial dynamics and brings new evidence for the understanding of fluvial risk management across

time. This transdisciplinary approach clarifies the multiscale parameters involved in the evolution of the Ostia paleomeander and identifies the successive redistribution of fluvial erosion along the riverbanks. During the Roman period, the combination of natural geomorphological processes and human pressures led to the formation of a compound meander near Ostia. This new river course constrained the development of Ostia to the east. As such, the Romans responded to this by displacing their infrastructure both locally (aqueduct and *Via Ostiensis*) and regionally (construction of Portus and excavation of the canals).

According to our hypothesis, clayey deposits in the riverbank and/or the massive Republican structure at the apex of the meander caused the formation of secondary lobes that subsequently redistributed the fluvial erosion upstream. From late Antiquity to the cut-off of the meander, the southern part of the meander of Ostia was stable and the urban area of the *Borgo* and the Castle of Giulio 2 remained safe even though they were located on the concave riverbank. A large flood occurring in AD 1557 initiated the cut-off of the meander and stopped definitively the lateral mobility of the paleomeander. Since then, the new river channel considerably eroded the archaeological site of Ostia at the north of the *Capitolium* - *Castrum*.

This active fluvial erosion in northern Ostia began during the *Rinascimento*, with the revival of Roman antiquity in Italy. However, the current acceptation of the concepts of cultural heritage and fluvial risk did not apply at that time. The two concepts originated in the 19th century (Segarra Lagunes, 2004; Combe, 2007). Fluvial risk management started in Rome when it became the capital of unified Italy (1871) and after several major floods of the

Tiber occurring in the middle of the 19th century. In this context, embankments were built in Rome along the Tiber River (*muraglioni)* and, five decades later, embankments were built in the Tiber Delta (Segarra Lagunes, 2004). Since the beginning of the 19th century, the archaeological site of Ostia has been studied by archaeologists (Fea, 1802, 1835; Canina, 1838; Vaglieri, 1909), and Carlo Fea, Director General of Antiquities, helped to control the random excavations and the trade of antiquities in Rome and Ostia (Ridley, 2000). Today, for Western societies, the concept of risk management extends not only to population and economically and socially viable infrastructures, but also toward cultural heritage preservation. Coastal erosion and its effects on archaeological sites have been recently taken into account in Italy (Lollino & Pagliarulo, 2008; Gerolamo, 2012). This work contributes to the consideration of fluvial damage to archaeological contexts.

More generally, the geoarchaeolocial approach can complete the picture of the risks prevailing for a river system and it can also identify the risks occurring in extreme conditions experienced at some point in the past (Thorndycraft et al., 2003; Bravard, 2004; Kidder et al., 2012). The big pebbles measured in the bedload of the paleomeander of Ostia and the destructive summer flash-flood of AD 1557 are evidence of exceptional fluvial events of the Tiber River. This question is particularly relevant to the beginning of the 21st century in which we are experiencing a climatic change and an increase of natural hazards.

ACKNOWLEDGMENTS

We would like to express our gratitude to the Soprintendenza Speciale per i Beni Archeologici di Roma, Donna Livia Aldobrandini, for access to the lands for corings. We would also like to thank Sabrina Zampini for the analysis of the pot shards found in the core

drillings. We are very grateful to the two anonymous reviewers and the editors for their very helpful comments for improving this paper. Thanks to ANR PolTevere (ANR-11-JSH3-0002), *Ecole française de Rome* and ERC-ROMP-PortusLimen (ERC grant number: 339123 - http://cordis.europa.eu/project/rcn/111587_en.html - www.portuslimen.eu). A special thank you to Peter Wheeler and Christina Triantafillou for the correction of the English, and Prof. Jean-Paul Bravard for his expert advice on fluvial dynamics and alluvial geoarchaeology.

REFERENCE CITED

Aldrete, G. S. (2007). Floods of the Tiber in ancient Rome. Baltimore: The Johns Hopkins University Press.

Allinne, C. (2007). Les villes romaines face aux inondations. La place des données archéologiques dans l'étude des risques fluviaux. Géomorphologie: relief, processus, environnement, 1/2007, 67–84.

Amenduni, G. (1884). Sulle opere di bonificazione della plaga litoranea dell'Agro Romano che comprende le paludi e gli stagni di Ostia, Porto, Maccarese e delle terre vallive di Stracciacappa, Baccano, Pantano e Lago dei Tartari. Relazione del progetto generale, 15, 36.

Amorosi, A., & Milli, S. (2001). Late Quaternary depositional architecture of Po and Tevere river deltas (Italy) and worldwide comparison with coeval deltaic successions. Sedimentary Geology, 144, 357–375.

Anwar, Y. M., El Askary, M. A., & Frihy, O. E. (1984). Reconstruction of sedimentary environments of Rosetta and Damietta promontories in Egypt, based on textural analysis. Journal of African Earth Sciences, 2, 17–29.

Arnaud-Fassetta, G. (2008). La géoarchéologie fluviale. EchoGéo [Online], 4/2008, URL : http://echogeo.revues.org/2187; DOI: 10.4000/echogeo.2187

Arnaud-Fassetta, G., Astrade, L., Bardou, É., Corbonnois, J., Delahaye, D., Fort, M., Gautier, E., Jacob, N., Peiry, J.-L., Piégay, H., & Penven, M.-J. (2009). Fluvial geomorphology and flood-risk management. Géomorphologie : relief, processus, environnement, 109–128.

Arnaud-Fassetta, G., Carcaud, N., Castanet, C., & Salvador, P.-G. (2010). Fluviatile palaeoenvironments in archaeological context: Geographical position, methodological approach and global change – Hydrological risk issues. Quaternary International, 216, 93–117.

Arnaud-Fassetta, G., & Landuré, C. (2003). Hydroclimatic hazards, vulnerability of societies and fluvial risk in the Rhone Delta (Mediterranean France) from the Greek period to the Early Middle Ages. E. Fouache (ed.), "The Mediterranean World Environment and History. Elsevier, Paris, 51–76.

Arnaud-Fassetta, G., Quisserne, D., & Antonelli, C. (2003). Downstream grain-size distribution of surficial bed material and its hydro-geomorphological significance in a large and regulated river: the Rhône River in its delta area (France). Géomorphologie : relief, processus, environnement, 9, 33–49.

Arnoldus-Huyzendveld, A., & Paroli, L. (1995). Alcune considerazioni sullo sviluppo storico dell'ansa dell Tevere presso Ostia e sul porto-canale. Archeologia Laziale, 383–392.

Bacci, A. (1576). Del Tevere - Libri Tre. Venetia.

Ball, D. F. (1964). Loss-on-ignition as an estimate of organic matter and organic carbon in non-calcareous soils. Journal of Soil Science, 15, 84–92.

Bellotti, P., Calderoni, G., Carboni, M. G., Di Bella, L., Tortora, P., Valeri, P., & Zernitskaya, V. (2007). Late Quaternary landscape evolution of the Tiber River delta plain (Central Italy): new evidence from pollen data, biostratigraphy and 14C dating. Zeitschrift für Geomorphologie, 51, 505–534.

Bellotti, P., Calderoni, G., Di Rita, F., D'Orefice, M., D'Amico, C., Esu, D., Magri, D., Martinez, M. P., Tortora, P., & Valeri, P. (2011). The Tiber river delta plain (central Italy): Coastal evolution and implications for the ancient Ostia Roman settlement. The Holocene, 21, 1105–1116.

Bellotti, P., Carboni, M. G., Milli, S., Tortora, P., & Valeri, P. (1989). La piana deltizia del Fiume Tevere: analisi di facies ed ipotesi evolutiva dell'ultimo "low stand" glaciale all'attuale. Giornale di Geologia, 51, 71–91.

Bellotti, P., Milli, S., Tortora, P., & Valeri, P. (1995). Physical stratigraphy and sedimentology of the Late Pleistocene-Holocene Tiber Delta depositional sequence. Sedimentology, 42, 617–634.

Bersani, P. (2004). Tiber River at Rome: summer floods and considerations on the maximum historical discharge. Geologia Tecnica e Ambientale, 2, 24-68.

Bersani, P., & Amici, R. (1993). Il trasporto solido del fiume Tevere. Idrotecnica, 3, 165–176.

Bersani, P., & Bencivenga, M. (2001). Le Piene del Tevere a Roma dal V secolo a.C. all'anno 2000 (Servizio Idrografico e Mareografico Nazionale.). Rome: Presidenza del Consiglio dei Ministri Dipartimento per i Servizi Tecnici Nazionali.

Bradford, R. A., O'Sullivan, J. J., Van der Craats, I. M., Krywkow, J., Rotko, P., Aaltonen, J., Bonaiuto, M., Dominicis, S. D., Waylen, K., & Schelfaut, K. (2012). Risk perception–issues for flood management in Europe. Natural Hazards and Earth System Science, 12, 2299–2309.

Bravard, J.-P. (2004). Le risque d'inondation dans le bassin du Haut Rhône : quelques concepts revisités dans une perspective géohistorique. In Fleuves et marais (pp. 391–402). Aix-en-Provence: CTHS.

Bravard, J.-P., Burnouf, J., & Vérot, A. (1989). Géomorphologie et archéologie dans la région lyonnaise : questions et réponses d'un dialogue interdisciplinaire. Bulletin de la Société préhistorique française, 86, 429–440.

Bravard, J.-P., Le Bot-Helly, A., Helly, B., & Savay-Guerraz, H. (1990). Le site de Vienne (38), Saint-Romain-en-Gal (69) et Sainte-Colombe (69): l'évolution de la plaine alluviale du Rhône de l'âge du Fer à la fin de l'Antiquité, proposition d'interprétation. Actes des Xe Rencontres

Internationales d'Archéologie et d'Histoire d'Antibes (19-21 octobre 1989), Archéologie et espaces. Éditions ADPCA, Juan-les-Pins, 437–452.

Bravard, J.-P., Provansal, M., Arnaud-Fassetta, G., Chabbert, S., Gaydou, P., Dufour, S., Richard, F., Valleteau, S., Melun, G., & Passy, P. (2008). Un atlas du paléo-environnement de la plaine alluviale du Rhône de la frontière suisse à la mer. Collections EDYTEM, 101–116.

Brown, A. G. (1997). Alluvial geoarchaeology: floodplain archaeology and environmental change. Cambridge: Cambridge University Press.

Bukowiecki, É., Dessales, H., & Dubouloz, J. (2008). Ostie, l'eau dans la ville: châteaux d'eau et réseau d'adduction. Rome: École française de Rome.

Cailleux, A., & Tricart, J. (1959). Initiation à l'étude des sables et des galets. Paris: Centre de documentation universitaire.

Calenda, G., Mancini, C. P., & Volpi, E. (2009). Selection of the probabilistic model of extreme floods: The case of the River Tiber in Rome. Journal of Hydrology, 371, 1–11.

Calza, G., Becatti, G., Gismondi, I., De Angelis D'Ossat, G., & Bloch, H. (1953). Scavi di Ostia, Topografia generale (Vol. 1). Roma: Libreria dello Stato.

Campbell, J. B. (2012). Rivers and the Power of Ancient Rome. Chapel Hill: University of North Carolina Press.

Camuffo, D., Bertolin, C., Schenal, P., Craievich, A., & Granziero, R. (2014). The Little Ice Age in Italy from documentary proxies and early instrumental records. Méditerranée. Revue géographique des pays méditerranéens / Journal of Mediterranean geography, 122, 17–30.

Camuffo, D., & Enzi, S. (1995). The analysis of two bi-millenary series: Tiber and Po River Floods. In Jones, P.D. Bradley, R.S. Jouzel, J. (Eds.), Climatic Variations and Forcing Mechanisms of the Last 2000 years (Vol. 41, pp. 433–450). Presented at the NATO ASI Series, Series I: Global Environmental Change, Stuttgart: Springer.

Canina, L. (1838). Sulla stazione delle navi di Ostia: sul porto di Claudio con le fosse indicate nella iscrizione scoperta l'anno 1836 e sul porto interno di Traiano e la fossa distinta col nome di questo imperatore. Atti della Pontificia Accademia romana di archeologia, 8, 257–310.

Capelli, G., & Mazza, R. (2008). Intrusione salina nel delta del fiume Tevere. Evoluzione del fenomeno nei primi anni del terzo millennio. In La geologia di Roma: dal Centro Storico alla Periferia - Seconda Parte (Vol. 80, pp. 237–260). Firenze: S.EL.C.A.

Combe, C. (2007). La ville endormie? Le risque d'inondation à Lyon. Approche géohistorique et systémique du risque de crue en milieu urbain et périurbain. Thèse de doctorat en géographie et aménagement, Université Lumière Lyon 2, Lyon.

De Angelis D'Ossat, G. (1938). Geo-pedogenesi delle terre sul delta del Tevere. Recherches sur le sol, 6, 138–168.

Dearing, J. A. (1999). Environmental magnetic susceptibility. Using the Bartington MS2 System, 32, 54.

Di Rita, F., Celant, A., & Magri, D. (2009). Holocene environmental instability in the wetland north of the Tiber delta (Rome, Italy): sea-lake-man interactions. Journal of Paleolimnology, 44, 51–67.

Doyle, L. J., & Garrels, R. M. (1985). What does percent organic carbon in sediments measure? Geo-Marine Letters, 5, 51–53.

Fea, C. (1802). Relazione: di un viaggio ad ostia e alla villa di Plinio detta Laurentino. Roma: Antonio Fulgoni Ed.

Fea, C. (1835). Il tevere navigabile oggidi come ne suoi piu antichi secoli e la citta d'Ostia ivi edificata dal re Anco Marcio emporio di Roma da risorgere a nuova vita. Rome: Nella Stamperia della Reverneda Camera Apostolica.

Folk, R. L., & Ward, W. C. (1957). Brazos River bar [Texas]; a study in the significance of grain size parameters. Journal of Sedimentary Research, 27, 3–26.Gerolamo, F. (Ed.). (2012). Erosione costiera in siti di interesse archeologico. Geologia dell'Ambiente, Supplemento al n. 1/2012, 0–46.

Giraudi, C. (2004). Evoluzione tardo-olocenica del delta del Tevere. Il Quaternario, 17, 477–492.

Giraudi, C. (2011). The sediments of the “Stagno di Maccarese” marsh (Tiber river delta, central Italy): A late-Holocene record of natural and human-induced environmental changes. The Holocene, 959683611405235, July 18, 1-11.

Giraudi, C., Tata, C., & Paroli, L. (2009). Late Holocene evolution of Tiber river delta and geoarchaeology of Claudius and Trajan Harbor, Rome. Geoarchaeology, 24, 371–382.

Goiran, J.-P., Salomon, F., Mazzini, I., Bravard, J.-P., Pleuger, E., Vittori, C., Boetto, G., Christiansen, J., Arnaud, P., Pellegrino, A., Pepe, C., & Sadori, L. (2014). Geoarchaeology confirms location of the ancient harbour basin of Ostia (Italy). Journal of Archaeological Science, 41, 389–398.

Goiran, J.-P., Tronchère, H., Collalelli, U., Salomon, F., & Djerbi, H. (2009). Découverte d’un niveau marin biologique sur les quais de Portus: le port antique de Rome. Méditerranée, 112, 59–67.

Goiran, J.-P., Tronchère, H., Salomon, F., Carbonel, P., Djerbi, H., & Ognard, C. (2010). Palaeoenvironmental reconstruction of the ancient harbors of Rome: Claudius and Trajan’s marine harbors on the Tiber delta. Quaternary International, 216, 3–13.

Hadler, H., Vött, A., Fischer, P., Ludwig, S., Heinzelmann, M., & Rohn, C. (2015). Temple-complex post-dates tsunami deposits found in the ancient harbour basin of Ostia (Rome, Italy). Journal of Archaeological Science, 61, 78–89.

Heinzelmann, M. (2001). Les nécropoles d’Ostie : topographie, développement, architecture, structure sociale. in Descoeudres, Ostie, port et porte de la Rome antique, musée Rath, Genève, 373–84.

Heinzelmann, M., & Martin, A. (2002). River port, navalia, and harbour temple at Ostia: new results of a DAI-AAR Project. Journal of roman archaeology, 15, 5–29.

Iadanza, C., & Napolitano, F. (2006). Sediment transport time series in the Tiber River. Physics and Chemistry of the Earth, Parts A/B/C, 31, 1212–1227.

Jin, D., & Schumm, S. A. (1986). A new technique for modelling river morphology. In Richards k.S. (ed), Proc. First Internat. Geomorphology Conf. (pp. 680–691). Chichester: Wiley.

Kasperson, J. X., Kasperson, R. E., Berberian, M., & Pacenka, L. A. (2005). The social contours of risk (Vol. 1). Earthscan London.

Keay, S., Millett, M., Paroli, L., & Strutt, K. (2005). Portus : An Archaeological Survey Of The Portus Of Imperial Rome. London: British School at Rome.

Keay, S., Parcak, S. H., & Strutt, K. D. (2014). High resolution space and ground-based remote sensing and implications for landscape archaeology: the case from Portus, Italy. Journal of Archaeological Science, 52, 277–292.

Kidder, T., Liu, H., Xu, Q., & Li, M. (2012). The Alluvial Geoarchaeology of the Sanyangzhuang Site on the Yellow River Floodplain, Henan Province, China. Geoarchaeology, 27, 324–343.

Le Gall, J. (1953). Le Tibre, fleuve de Rome dans l'antiquité. Paris: Presses Universitaires de France.

Leveau, P. (2008). Les inondations du Tibre à Rome: politiques publiques et variations climatiques à l'époque romaine. In Actes du colloque international de Québec (27-29 octobre 2006), La gestion intégrée des ressources en eau dans l'histoire environnementale: savoirs traditionnels et pratiques modernes. (pp. 137–146). Roma: "L'Erma" di Bretschneider.

Lollino, P., & Pagliarulo, R. (2008). The interplay of erosion, instability processes and cultural heritage at San Nicola Island (Tremiti Archipelago, Southern Italy). Geogr. Fis. Dinam. Quat, 31, 161–169.

Maillet, G. (2005). Relations sédimentaires récentes et actuelles entre un fleuve et son delta en milieu microtidal: Exemple de l'embouchure du Rhône (Thèse de géomorphologie). Université de Provence-Aix-Marseille I.

Martino, V. D., & Belati, M. (1980). Qui arrivò il Tevere. Le inondazioni del Tevere nelle testimonianze e nei ricordi storici. Rome: Multigrafica Editrice.

Miller, N. P. (1959). Tacitus: Annals Book I (Methuen & Co. Ltd.). London.

Milli, S. (1997). Depositional setting and high-frequency sequence stratigraphy of the Middle-Upper Pleistocene to Holocene deposits of the Roman Basin. Geologica Romana, 33, 99–136.

Milli, S., D'Ambrogi, C., Bellotti, P., Calderoni, G., Carboni, M. G., Celant, A., Di Bella, L., Di Rita, F., Frezza, V., Magri, D., Pichezzi, R. M., & Ricci, V. (2013). The transition from wave-dominated estuary to wave-dominated delta: The Late Quaternary stratigraphic architecture of Tiber River deltaic succession (Italy). Sedimentary Geology, 284–285, 159–180.

Pannuzi, S. (2009). Il Castello di Giulio II ad Ostia Antica. Firenze: Ed. All'Insegna del Giglio.

Pavolini, C. (2006). Ostia (Vols. 1-1). Roma ; Bari: G. Laterza.

Pellegrino, A., Olivanti, P., & Panariti, F. (1995). Ricerche archeologiche nel Trastevere Ostiense. Archeologia laziale, 12, 393–400.

Pepe, C., Sadori, L., Andrieu-Ponel, V., Salomon, F., & Goiran, J.-P. (2016). Late Holocene pollen record from Fiume Morto (Dead River), a palaeomeander of Tiber River near Ancient Ostia (central Italy). Journal of Paleolimnology.

Perès, J. M., & Picard, J. (1964). Nouveau manuel de bionomie benthique de la Mer Méditerranée (Vol. 47). Marseille: Rec. Trav. Station marine d'Endoume.

Reimer, P. J., Bard, E., Bayliss, A., Beck, J. W., Blackwell, P. G., Bronk Ramsey, C., Buck, C. E., Cheng, H., Edwards, R. L., Friedrich, M., Grootes, P. M., Guilderson, T. P., Haflidason, H., Hajdas, I., Hatté, C., Heaton, T. J., Hoffmann, D. L., Hogg, A. G., Hughen, K. A., Kaiser, K. F., Kromer, B., Manning, S. W., Niu, M., Reimer, R. W., Richards, D. A., Scott, E. M., Southon, J. R., Staff, R. A., Turney, C. S. M., & van der Plicht, J. (2013). IntCal13 and Marine13 radiocarbon age calibration curves 0-50,000 years cal BP. Radiocarbon, 55, 1869–1887.

Ridley, R. T. (2000). The pope's archaeologist: the life and times of Carlo Fea. Rome: Quasar.

Rosgen, D. L. (1994). A classification of natural rivers. Catena, 22, 169–199.

Salomon, F. (2013). Géoarchéologie du delta du Tibre : Evolution géomorphologique holocène et contraintes hydrosédimentaires dans le système Ostie - Portus (Thèse de doctorat en Géographie Physique / Géoarchéologie). Université Lyon 2.

Salomon, F., Delile, H., Goiran, J.-P., Bravard, J.-P., & Keay, S. (2012). The Canale di Comunicazione Traverso in Portus: the Roman sea harbour under river influence (Tiber delta, Italy). Géomorphologie : relief, processus, environnement, 75–90.

Salomon, F., Goiran, J.-P., Bravard, J.-P., Arnaud, P., Djerbi, H., Kay, S., & Keay, S. (2014). A harbour–canal at Portus: a geoarchaeological approach to the Canale Romano: Tiber delta, Italy. Water History, 6, 31–49.

Segarra Lagunes, M. M. (2004). Il Tevere e Roma: Storia di una simbiosi. Gangemi Editore.

Segre, A. G. (1986). Considerazioni sul Tevere e sull'Aniene nel Quaternario. In: Il Tevere e le altre vie d'acqua del Lazio antico. Archeologia Laziale, VII, 9–17.

Shepherd, E. J. (2006). Il "Rilievo Topofotografico di Osita dal Pallone." AArea II, 15–38.

Testaguzza, O. (1970). Portus: illustrazione dei Porti di Claudio e Traiano. Rome: Julia Editrice.

Thorndycraft, V. R., Benito, G., Llasat, M. C., & Barriendos, M. (2003). Palaeofloods, historical data & climatic variability: Applications in flood risk assessment. Madrid: Centro de Ciencias Medioambientales.

Vaglieri, D. (1909). Notizie di Scavi.

Van den Berg, J. H. (1995). Prediction of alluvial channel pattern of perennial rivers. Geomorphology, 12, 259–279.

Vittori, C., Mazzini, I., Salomon, F., Goiran, J.-P., Pannuzi, S., Rosa, C., & Pellegrino, A. (2015). Palaeoenvironmental evolution of the ancient lagoon of Ostia Antica (Tiber delta, Italy). Journal of Archaeological Science, 54, 374–384.

Zevi, F. (2001). Les débuts d'Ostie (pp. 3–9). Presented at the Descoeudres J.-P. (dir.), Ostia port et porte de Rome antique, Georg éditeur.

FIGURE CAPTIONS

Figure 1. Location map of study area. This figure shows the paleomeander of Ostia in its final morphology and the locations of boreholes MO1, 2 and 3. The limit of the lagoonal deposits near the paleomeander is drawn using the paleolagoon shape from Amenduni (Amenduni, 1884) and sedimentary data (De Angelis D'Ossat, 1938).

Figure 2. Morphometric characteristics of the paleomeander, archaeological data, and core locations.

Figure 3. Stratigraphic descriptions of Core MO3 (convexity of the Ostia paleomeander).

Figure 4. Stratigraphic descriptions of Core MO1 (channel of the Ostia paleomeander).

Figure 5. Stratigraphic descriptions of of Core MO2 (concavity of the Ostia paleomeander).

Figure 6. Interpretative cross-section of the Ostia meander paleochannel.

Figure 7. Four maps showing the evolution of the paleomeander in relation to the city of Ostia.

Figure 1

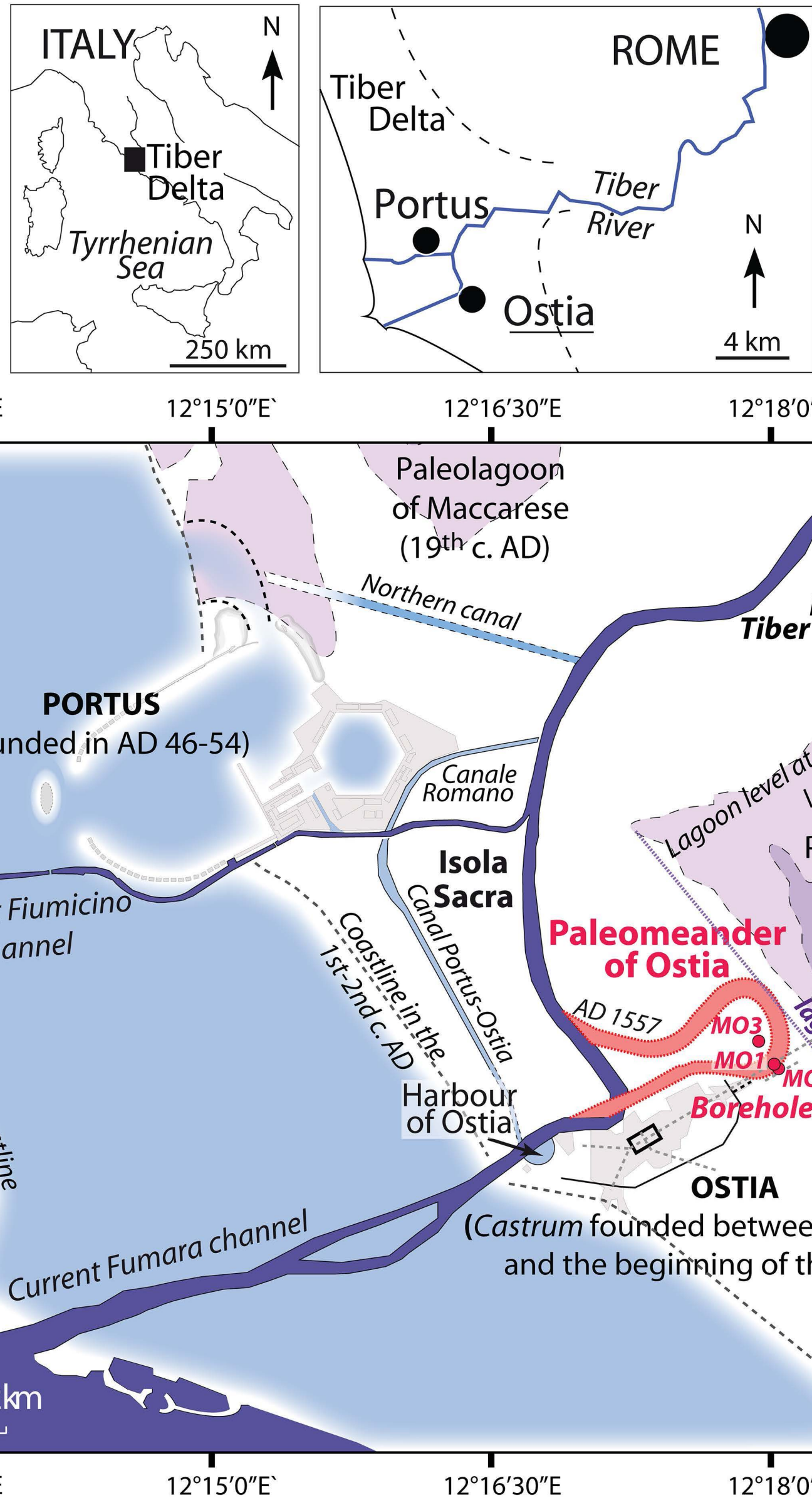
ITALY
N
Tiber Delta
Tyrrhenian Sea
250 km
ROME
Tiber Delta
Portus
Tiber River
Ostia
N
4 km
12°13′30″E
12°15′0″E`
12°16′30″E
12°18′0″E
12°19′30″E
41°48′0″N
41°46′30″N
41°45′0″N
N
Paleolagoon of Maccarese (19th c. AD)
Current Tiber channel
Northern canal
Holocene Tiber delta deposits
Pleistocene deposits
PORTUS
(founded in AD 46-54)
Canale Romano
Lagoon level at +0.80 m
Lagoon level at +0.40 m
Isola Sacra
Paleolagoon of Ostia (19th c. AD)
Via Ostiensis
Current Fiumicino channel
Coastline in the 1st-2nd c. AD
Canal Portus-Ostia
Paleomeander of Ostia
AD 1557
MO3
MO1
MO2
Boreholes
Lagoonal deposits
Limit of the
Harbour of Ostia
Current coastline
OSTIA
(Castrum founded between the 4th c. BC and the beginning of the 3rd c. BC)
Tyrrhenian sea
Current Fumara channel
0
2km

Figure 2

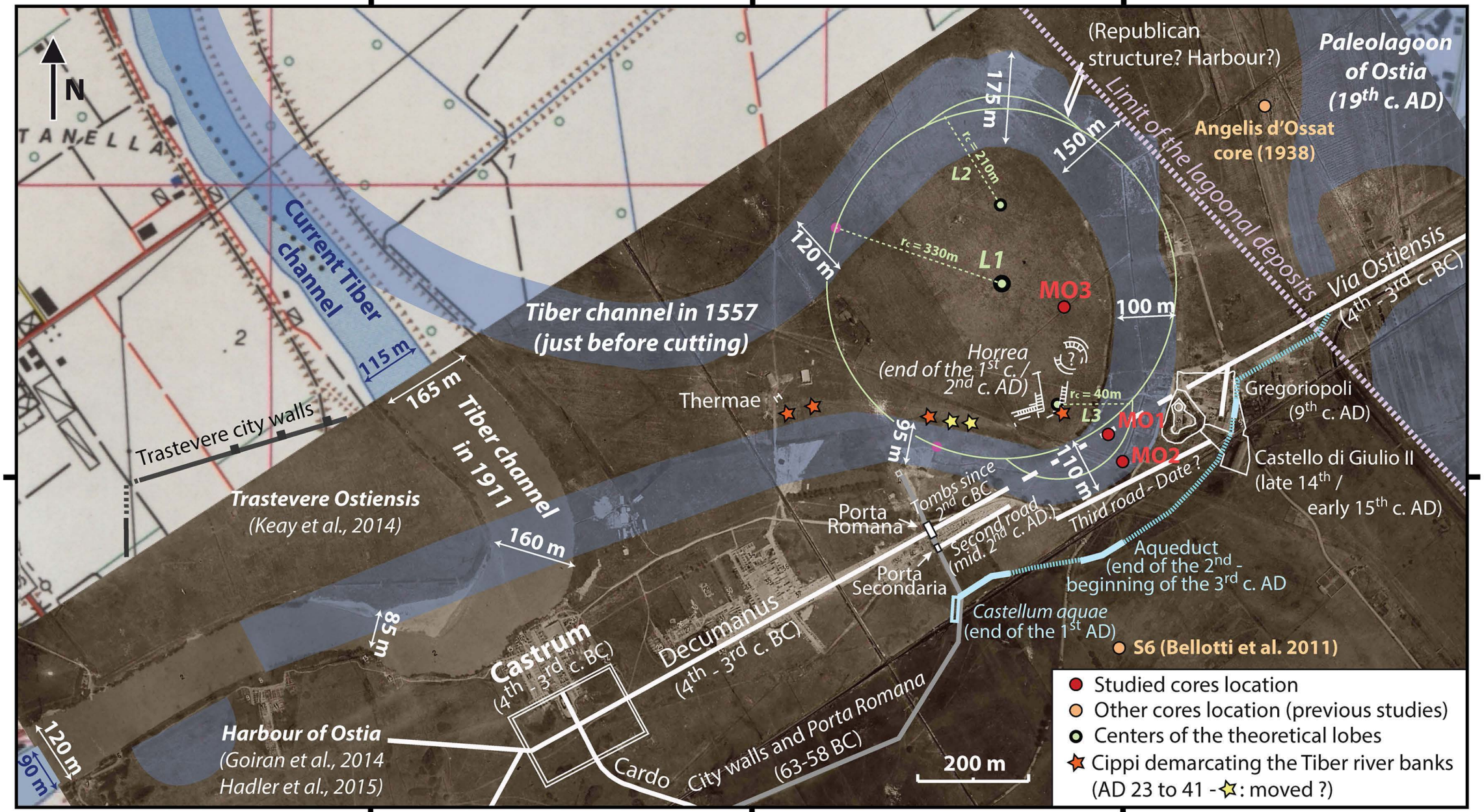
12°17′0″E
12°17′30″E
12°18′0″E
41°45′30″N
N
Current Tiber channel
115 m
Tiber channel in 1557 (just before cutting)
165 m
Tiber channel in 1911
160 m
85 m
120 m
90 m
Trastevere city walls
Trastevere Ostiensis (Keay et al., 2014)
Harbour of Ostia (Goiran et al., 2014 Hadler et al., 2015)
Castrum (4th - 3rd c. BC)
Decumanus (4th - 3rd c. BC)
Cardo
City walls and Porta Romana (63-58 BC)
Thermae
Horrea (end of the 1st c. / 2nd c. AD)
Porta Romana
Porta Secondaria
Tombs since 2nd c BC
Second road (mid. 2nd c. AD.)
Third road - Date ?
Aqueduct (end of the 2nd - beginning of the 3rd c. AD
Castellum aquae (end of the 1st AD)
S6 (Bellotti et al. 2011)
(Republican structure? Harbour?)
175 m
150 m
rc = 210m
L2
120 m
rc = 330m
L1
MO3
100 m
95 m
rc = 40m
L3
MO1
MO2
110 m
Limit of the lagoonal deposits
Paleolagoon of Ostia (19th c. AD)
Angelis d'Ossat core (1938)
Via Ostiensis (4th - 3rd c. BC)
Gregoriopoli (9th c. AD)
Castello di Giulio II (late 14th / early 15th c. AD)
200 m
Studied cores location
Other cores location (previous studies)
Centers of the theoretical lobes
Cippi demarcating the Tiber river banks (AD 23 to 41 - ☆: moved ?)

Figure 3

Core MO3 - Analysis

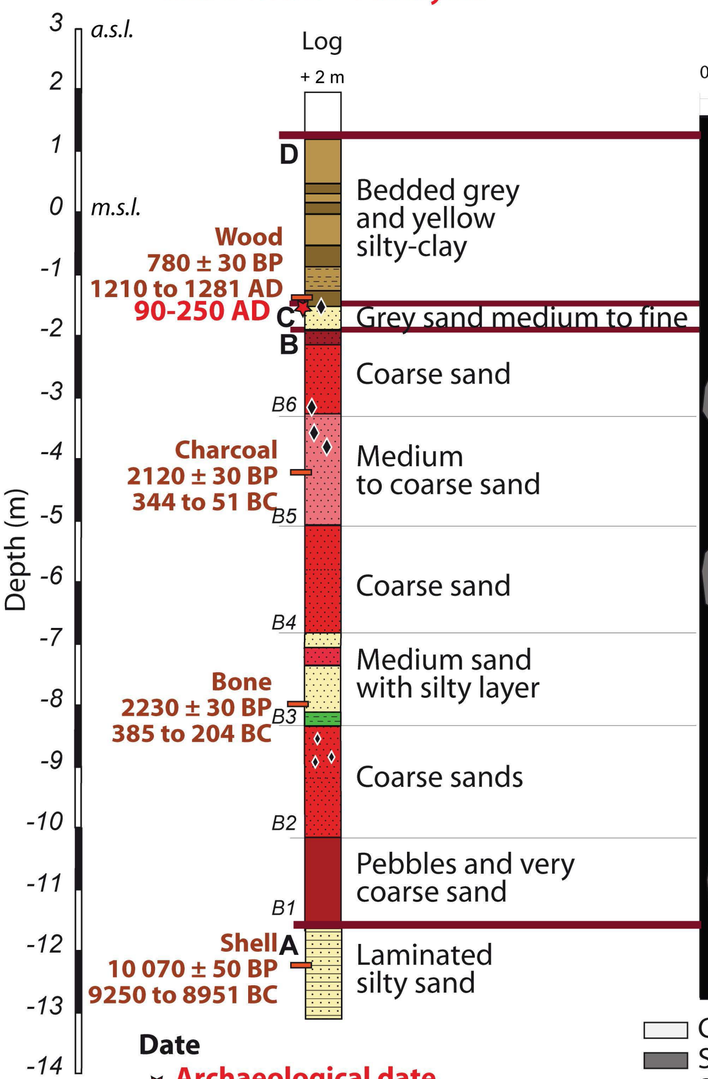

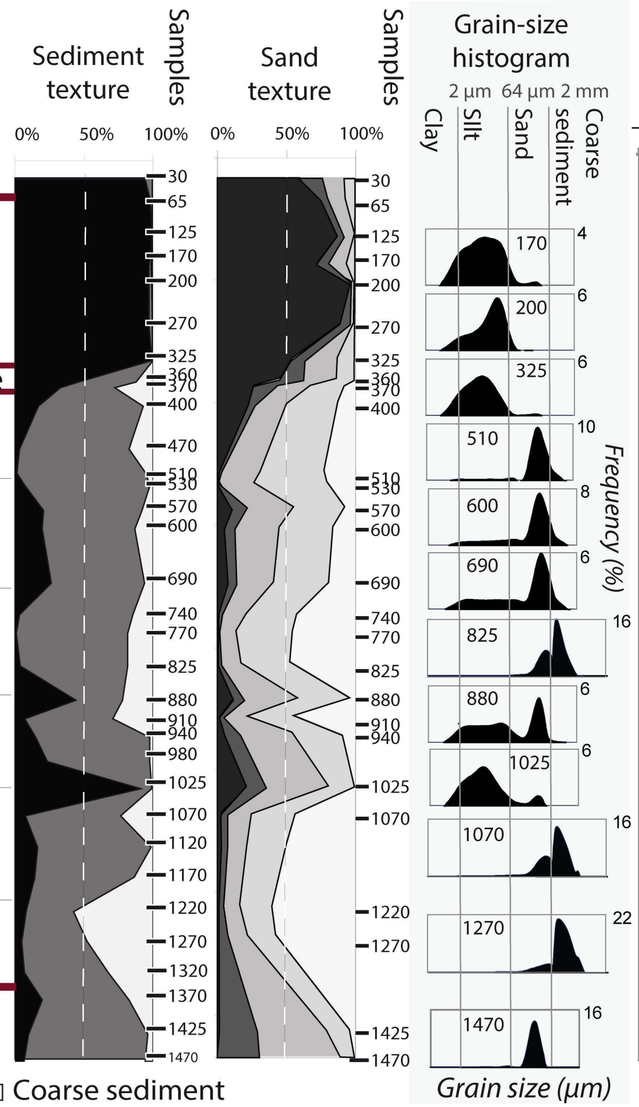

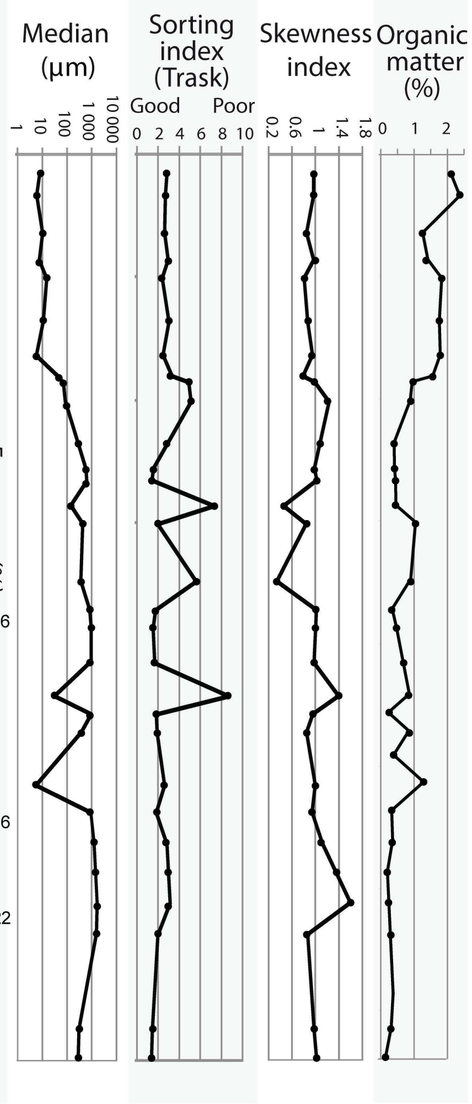

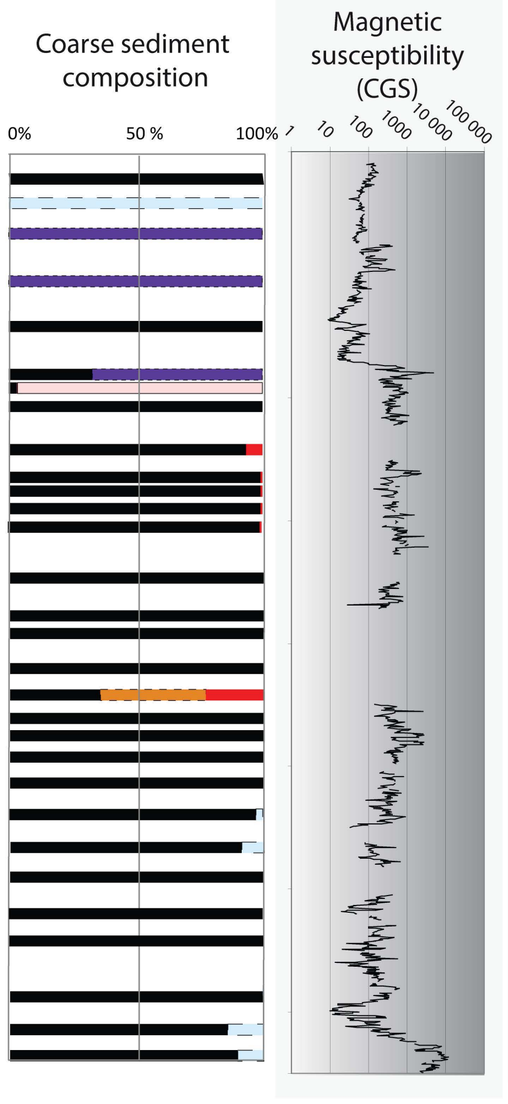

INTERPRETATIONS

FLOODPLAIN DEPOSITS

ANTHROPIC STRATA

POINT BAR SYSTEM

Lower energy in the point bar construction

POINT BAR SYSTEM

DELTAIC BEACH-RIDGE SYSTEM

Date

- Archaeological date (ceramics)
- Radiocarbon date

Stratigraphy

- Pebbles and very coarse sand
- Very coarse sand, coarse sand
- Medium, fine and silty sand
- Grey silty clay, clayey silt
- Yellow/grey silty clay
- Ceramics

- Coarse sediment
- Sand
- Silt and clay

- Very coarse sand (1000 to 1600 µm)
- Coarse sand (500 to 1000 µm)
- Medium sand (250 to 500 µm)
- Fine sand (125 to 250 µm)
- Very fine sand (63 to 125 µm)

- Rudites
- Tuff
- Shells
- No coarse sediment
- Concretions
- Mortar
- Ceramics

Figure 4

Core MO1 - Analysis

Log

Sediment texture

Sand texture

Grain-size histogram

Median (µm)

Sorting index (Trask)

Organic matter (%)

Coarse sediment composition

Magnetic susceptibility (CGS)

INTERPRETATIONS

Depth (m)

a.s.l.

m.s.l.

+ 1.79 m

Current times

E — Grey laminated silty clay

E2

Grey clayey silts

E1

D — Grey silty sand

D2

Medium sands

D1

C — Coarse to very coarse sands

Bone
355 ± 25 BP
1454 to 1634 AD

B — *Tuff* Pebbles, very coarse

B4 — *Tuff* sands and tuff

B3 — Laminated medium sand

B2 — Medium sand

B1 — Pebbles and very coarse sands

A — Laminated silty sand

Samples

Good — Poor

2 µm — 64 µm — 2 mm

Clay — Silt — Sand — Coarse sediment

Frequency (%)

OXBOW LAKE

CUT OFF CHANNEL INFILL

BEDLOAD 3

BEDLOAD2

Riverbanks erosion / bedload deposits?

BEDLOAD 1

DELTAIC BEACH-RIDGE SYSTEM

Date

Radiocarbon date

Stratigraphy

- Pebbles and very coarse sand
- Very coarse sand, coarse sand
- Medium, fine and silty sand
- Grey silty clay, clayey silt
- Tuff
- Ceramics

- Coarse sediment
- Sand
- Silt and clay

Grain size (µm)

- Very coarse sand (1000 to 1600 µm)
- Coarse sand (500 to 1000 µm)
- Medium sand (250 to 500 µm)
- Fine sand (125 to 250 µm)
- Very fine sand (63 to 125 µm)

- Rudites
- Concretions
- Tuff
- Ceramics
- Shells
- No coarse sediment

Core MO2 - Analysis

Figure 5

Log

Depth (m)

a.s.l.

m.s.l.

+ 1.70 m

Current times

D

Grey silty-clay

Wood
2035± 30 BP
159 BC to 50 AD

C

Grey silty-clay

C3

Wood
2160 ± 25 BP
356 to 112 BC

Medium sand

C2

C1

Grey silty-clay

B

Very coarse to coarse sands

B2

B1

Pebbles and sands

A

Laminated silty sand

Sediment texture

Sand texture

0% 50% 100%

Samples

Grain-size histogram

2 µm 64 µm 2 mm

Clay Silt Sand Coarse sediment

Frequency (%)

Grain size (µm)

Median (µm)

0 200 400 600 800

Sorting index (Trask)

Good Poor

0 4 8

Organic matter (%)

0.1 1 10

Coarse sediment composition

0% 50 % 100%

Magnetic susceptibility (CGS)

1 10 100 1000 10 000

INTERPRETATIONS

OXBOW LAKE

CUT OFF CHANNEL INFILL

Riverbank erosion, beadload deposit and flocculation

BEDLOAD

DELTAIC BEACH-RIDGE SYSTEM

Date

Radiocarbon date

Stratigraphy

- Pebbles and very coarse sand
- Very coarse sand, coarse sand
- Medium, fine and silty sand
- Grey silty clay, clayey silt
- Yellow/grey silty clay
- Ceramics

- Coarse sediment
- Sand
- Silt and clay

- Very coarse sand (1000 to 1600 µm)
- Coarse sand (500 to 1000 µm)
- Medium sand (250 to 500 µm)
- Fine sand (125 to 250 µm)
- Very fine sand (63 to 125 µm)

- Rudites
- Tuff
- Shells
- No coarse sediment
- Concretions
- Ceramics

Figure 6

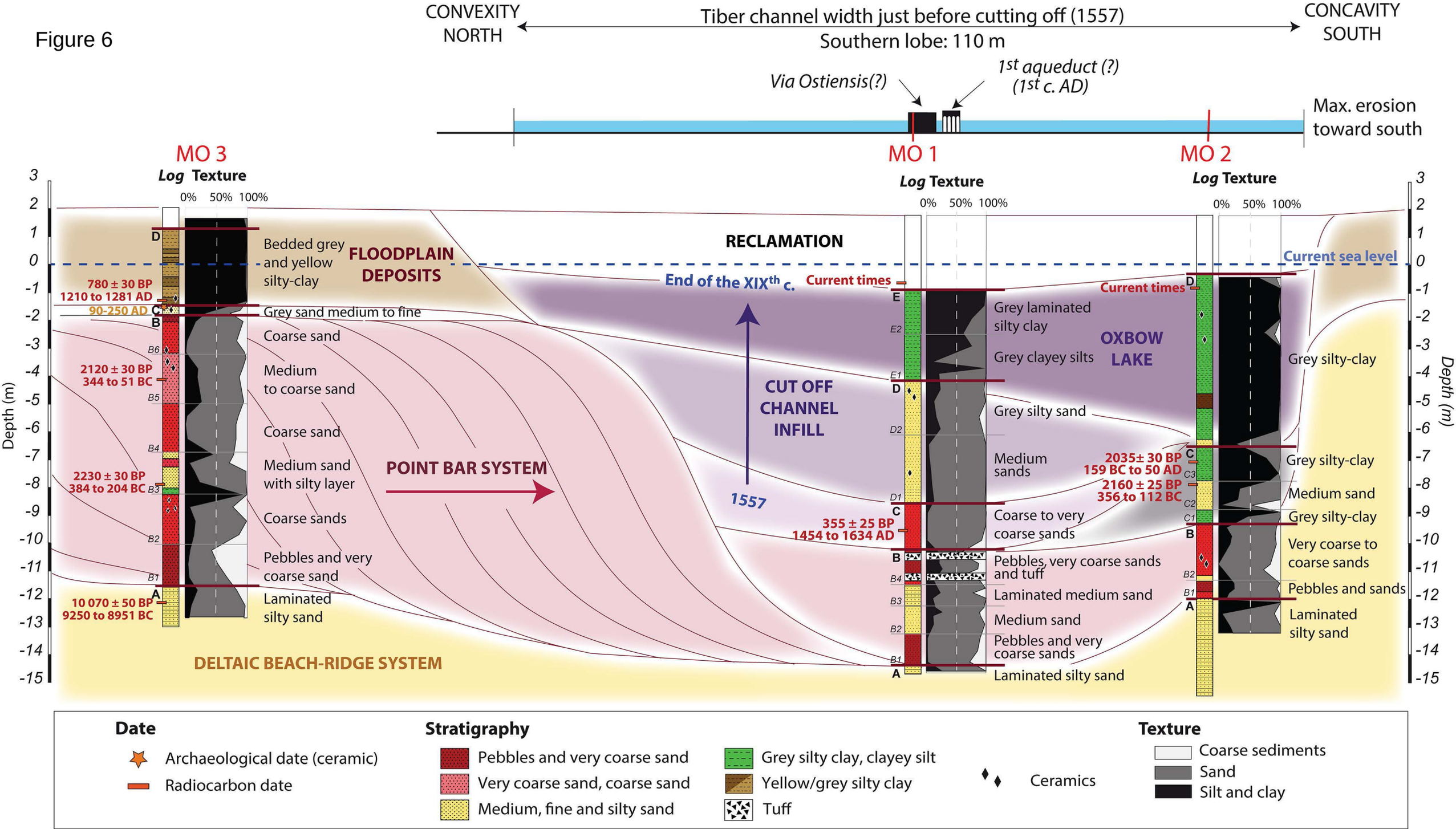
CONVEXITY NORTH
Tiber channel width just before cutting off (1557)
Southern lobe: 110 m
CONCAVITY SOUTH
Via Ostiensis(?)
1st aqueduct (?) (1st c. AD)
Max. erosion toward south
MO 3
MO 1
MO 2
Log Texture
0% 50% 100%
Depth (m)
RECLAMATION
End of the XIXth c.
Current times
Current sea level
FLOODPLAIN DEPOSITS
Bedded grey and yellow silty-clay
780 ± 30 BP
1210 to 1281 AD
90-250 AD
Grey sand medium to fine
Coarse sand
Medium to coarse sand
2120 ± 30 BP
344 to 51 BC
Coarse sand
Medium sand with silty layer
2230 ± 30 BP
384 to 204 BC
Coarse sands
Pebbles and very coarse sand
10 070 ± 50 BP
9250 to 8951 BC
Laminated silty sand
POINT BAR SYSTEM
CUT OFF CHANNEL INFILL
1557
OXBOW LAKE
Grey laminated silty clay
Grey clayey silts
Grey silty sand
Medium sands
355 ± 25 BP
1454 to 1634 AD
Coarse to very coarse sands
Pebbles, very coarse sands and tuff
Laminated medium sand
Medium sand
Pebbles and very coarse sands
Laminated silty sand
2035± 30 BP
159 BC to 50 AD
2160 ± 25 BP
356 to 112 BC
Grey silty-clay
Medium sand
Grey silty-clay
Very coarse to coarse sands
Pebbles and sands
Laminated silty sand
DELTAIC BEACH-RIDGE SYSTEM
Date
Archaeological date (ceramic)
Radiocarbon date
Stratigraphy
Pebbles and very coarse sand
Very coarse sand, coarse sand
Medium, fine and silty sand
Grey silty clay, clayey silt
Yellow/grey silty clay
Tuff
Ceramics
Texture
Coarse sediments
Sand
Silt and clay

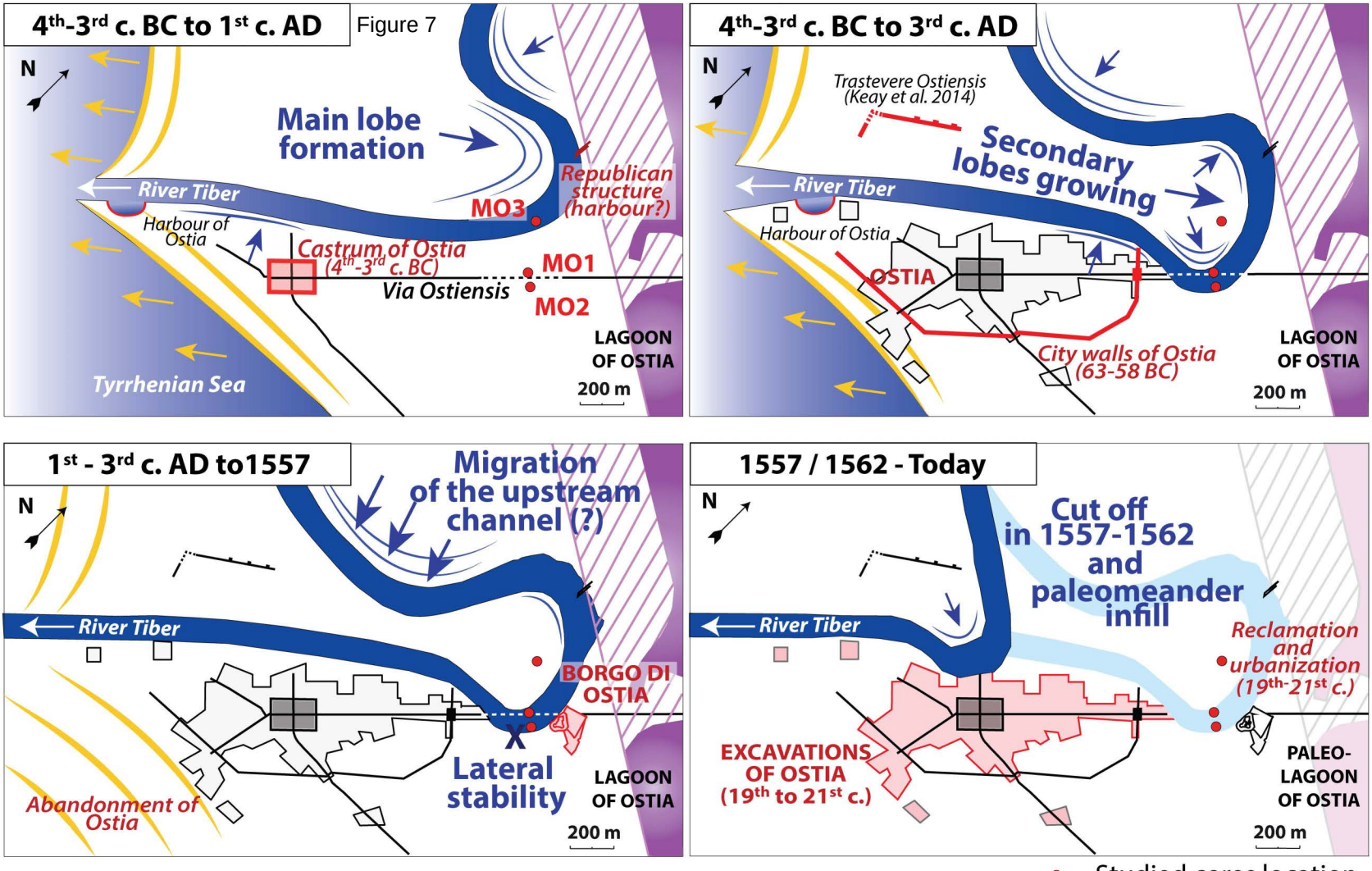
4th-3rd c. BC to 1st c. AD
Figure 7
N
Main lobe formation
River Tiber
Harbour of Ostia
Castrum of Ostia (4th-3rd c. BC)
MO3
MO1
MO2
Via Ostiensis
Republican structure (harbour?)
Tyrrhenian Sea
LAGOON OF OSTIA
200 m
4th-3rd c. BC to 3rd c. AD
N
Trastevere Ostiensis (Keay et al. 2014)
Secondary lobes growing
River Tiber
Harbour of Ostia
OSTIA
City walls of Ostia (63-58 BC)
LAGOON OF OSTIA
200 m
1st - 3rd c. AD to1557
N
Migration of the upstream channel (?)
River Tiber
BORGO DI OSTIA
Lateral stability
Abandonment of Ostia
LAGOON OF OSTIA
200 m
1557 / 1562 - Today
N
Cut off in 1557-1562 and paleomeander infill
River Tiber
Reclamation and urbanization (19th-21st c.)
EXCAVATIONS OF OSTIA (19th to 21st c.)
PALEO-LAGOON OF OSTIA
200 m
Studied cores location

Table 1

Radiocarbon date – ARTEMIS program – Lyon - France					
Samples (Depth related to the Core Depth)	**Laboratory samples**	**Sample description**	**Activity (in %)**	**Radiocarbon Age (^{14}C yr BP)**	**2σ calibrated Age (Reimer et al., 2013)**
MO-1 / 9.64m	Ly-8041	Bone	95.654 ± 0.270	355 ± 25	AD 1454 to 1634
MO-1 / 0.76m	Ly-8040	Organic matter	103.210 ± 0.278	Today	
MO-2 / 7.18m	Ly-8780	Wood	77.612 ± 0.243	2035 ± 30	159 BC to AD 50
MO-2 / 0.9m	Ly-8788	Wood	106.635 ± 0.329	Today	
MO-2 / 8m	Ly-8044	Wood	76.430 ± 0.244	2160 ± 25	356 to 112 BC
MO-3 / 8m	Ly-8792	Bone	75.751 ± 0.287	2230 ± 30	384 to 204 BC
MO-3 / 12.25 m	Ly-8799	Shell	28.546 ± 0.172	10 070 ± 50	9250 to 8951 BC*
MO-3 / 1.35 m	Ly-8781	Wood	90.762 ± 0.294	780 ± 30	AD 1210 to 1281
MO-3 / 4m	Ly-8793	Charcoal	76.802 ± 0.262	2120 ± 30	344 to 51 BC
Archaeological date					
Core	**Location**	**Ceramic**		**Archaeological date**	**Identification**
MO3-Unit C	Paleomeander of Ostia - Convexity	Terra sigillata “Africana A”		90-250 AD	S. Zampini (ceramologist – pers. comm.)

Radiocarbon, and archaeological ages.* ***Calibrated using the Marine13 curve***